Three-dimensional electron momentum densities: A comparison of $(\gamma,e\gamma)$ and $(e,2e)$ spectroscopies

F. F. Kurp*
Hamburger Synchrotronstrahlungslabor (HASYLAB) at Deutsches Elektronen-Synchrotron (DESY), Notkestrasse 85, 22603 Hamburg, Germany

M. Vos
Electronic Structure of Materials Centre, Flinders University of South Australia, G.P.O. Box 2100, Adelaide, South Australia, 5001, Australia

Th. Tschentscher
European Synchrotron Radiation Facility, Boîte Postale 220, 38043 Grenoble, France

A. S. Kheifets
Electronic Structure of Materials Centre, Flinders University of South Australia, G.P.O. Box 2100, Adelaide, South Australia, 5001, Australia

J. R. Schneider
Hamburger Synchrotronstrahlungslabor (HASYLAB) at Deutsches Elektronen-Synchrotron (DESY), Notkestrasse 85, 22603 Hamburg, Germany

E. Weigold†
Electronic Structure of Materials Centre, Flinders University of South Australia, G.P.O. Box 2100, Adelaide, South Australia, 5001, Australia

F. Bell
Sektion Physik, Universität München, Am Coulombwall 1, 85748 Garching, Germany
(Received 3 September 1996)

We report on the comparison of a $(\gamma,e\gamma)$ with an $(e,2e)$ experiment made with the same 17-nm thin graphite foil. The energies of the projectile, scattered projectile, and recoil electron were 174.5, 108.9, and 65.6 keV in the case of the $(\gamma,e\gamma)$ experiment and 20, 18.8, and 1.2 keV for the $(e,2e)$ study. In the coincident $(e,2e)$ energy-loss spectra, two distinct peaks are observed which are attributed to σ and π electrons. If the spectral momentum density of the $(e,2e)$ experiment is integrated over the energy loss, the resulting momentum density can be compared directly with the $(\gamma,e\gamma)$ result. Good overall agreement is observed between both methods and the resulting three-dimensional electron momentum density is well reproduced by both a pseudopotential and density-functional calculation. The remaining differences between the $(e,2e)$ and $(\gamma,e\gamma)$ results are discussed in terms of multiple elastic electron scattering, which might affect the $(e,2e)$ data. [S0163-1829(97)05908-0]

I. INTRODUCTION

Overwhelming interest in the electronic structure of solids led to the development of a large variety of experimental methods of studying the energy dispersion and density of states for both the occupied and unoccupied bands: angle-resolved inverse photoemission[1] and photoelectron emission,[2] inelastic x-ray scattering,[3] electron-energy-loss spectroscopy,[4] and x-ray-absorption spectroscopy,[5] to name but a few. In contrast, there exist only a few methods that measure more-or-less directly wave-function-related quantities such as real-space electron density (x-ray form factors) (Ref. 6) or momentum densities. To the latter belong positron-annihilation experiments[7]—which, strictly speaking, measure the electron-positron pair density, i.e., the momentum density weighted by the positron wave function within the solid[8]—and $(\gamma,e\gamma)$ and $(e,2e)$ spectroscopy. It is the aim of this paper to present a comparative study of these methods of spectroscopy. Suppose that a high-energy projectile (a photon or an electron) is scattered by an electron at rest. For fixed scattering angles both the energy of the scattered projectile and of the recoil electron will be sharp. In contrast, in the case of moving electrons, both particles in the final state will suffer a kind of Doppler broadening yielding energy distributions for the scattered radiation. In addition, if the scattered projectile and the recoil electron are measured *in coincidence*, the scattering kinematics are fixed, which allows the reconstruction of the initial electron momentum in a unique way. The coincidence count rate will be proportional to the electron-momentum density (EMD). Consequently, the technique has been called ''wave-function mapping.''[9] Up to now, this idea has been successfully ap-

plied to the evaluation of the EMD of solids by using either a photon or an electron as the projectile. In the former case, the technique has been named $(\gamma,e\gamma)$-, in the latter $(e,2e)$-, or electron-momentum spectroscopy.[9–13] Though both types of experiments yield the same information—the EMD of a solid—the experimental details are rather different, leading to advantages and disadvantages if the methods are compared. The most severe problem for both experiments is the disturbance of the recoil electron due to multiple elastic or inelastic scattering within the solid target. This kind of scattering introduces a smearing of both the final momentum and the energy of the electron which affects the determination of the EMD. Thus, inevitably very thin target foils with thicknesses comparable to the mean free path for scattering have to be used in order to minimize this problem. Comparing $(\gamma,e\gamma)$ and $(e,2e)$ experiments, the situation is more relaxed in the former case, since at least the photon will not be multiply scattered. The big advantage of the $(e,2e)$ technique is its large intrinsic cross section and the high monochromatic projectile flux, which can be achieved easily. For the experimental situation described below, we obtain from the Møller cross section 13 kb/sr/electron for the $(e,2e)$ experiment (20 keV primary electron energy, 14° scattering angle), whereas the Klein-Nishina cross section yields only 29 mb/sr/electron (175 keV photon energy, 140° scattering angle), giving a factor of 5×10^5 in favor of the $(e,2e)$ experiment. In addition, a highly monochromatic electron flux of 10^{12} electrons/s ($\sim$100 nA) is easily achieved, whereas comparable photon fluxes with considerably less monochromaticity are obtained only from synchrotron radiation facilities of the third generation. Altogether, this allows the use of electron spectrometers in $(e,2e)$ experiments, which, in turn, makes it possible to measure the EMD of solids as a function of the valence binding energy with a resolution of about 1.0 eV.

In the following we compare a $(\gamma,e\gamma)$ with an $(e,2e)$ experiment where the same target has been used. The experiments have been made, respectively, at the European Synchrotron Radiation Facility (ESRF) in Grenoble, France, and at the Electronic Structure of Materials Centre in Adelaide, Australia.

II. METHOD

Consider a projectile with energy E_0 and momentum $\mathbf{p}_0$ which is scattered at a target electron with initial momentum $\mathbf{q}$ resulting in a scattered projectile with energy E_s and momentum $\mathbf{p_s}$. The recoil electron will acquire momentum $\mathbf{p_r}$ and energy E_r. If the electron was bound with an energy $\epsilon>0$ relative to the vacuum level, the following relations hold:

$$\epsilon=E_0-E_s-E_r\,,\qquad \mathbf{q}=\mathbf{p}_s+\mathbf{p}_r-\mathbf{p}_0\,. \tag{1}$$

If all the momenta and energies are fixed experimentally, $\mathbf{q}$ and ϵ can be reconstructed in a unique way. Assuming the validity of the impulse approximation,[13,14] the coincidence count rate will be proportional to the spectral electron momentum density (SEMD) $\rho_j(\epsilon,\mathbf{q})=\rho_j(\mathbf{q})\delta[\epsilon-\epsilon_j(\mathbf{q})]$, where $\rho_j(\mathbf{q})$ is the EMD of the jth band. In a crystalline solid, the binding energy and momentum are correlated through the dispersion relation $\epsilon=\epsilon_j(\mathbf{q})$, where, in the extended-zone scheme, $\mathbf{q}=\mathbf{k}+\mathbf{g}$. $\mathbf{k}$ is the crystal momentum (i.e., restricted to the 1. Brillouin zone) and $\mathbf{g}$ a reciprocal-lattice vector. Whereas in the $(e,2e)$ experiment to be described, the energy resolution is good enough to measure the SEMD for the separate valence-electron bands and core electrons,[15] the $(\gamma,e\gamma)$ experiment integrates over all binding energies, thus yielding the EMD $\rho(\mathbf{q})$ summed over all bands and binding energies.

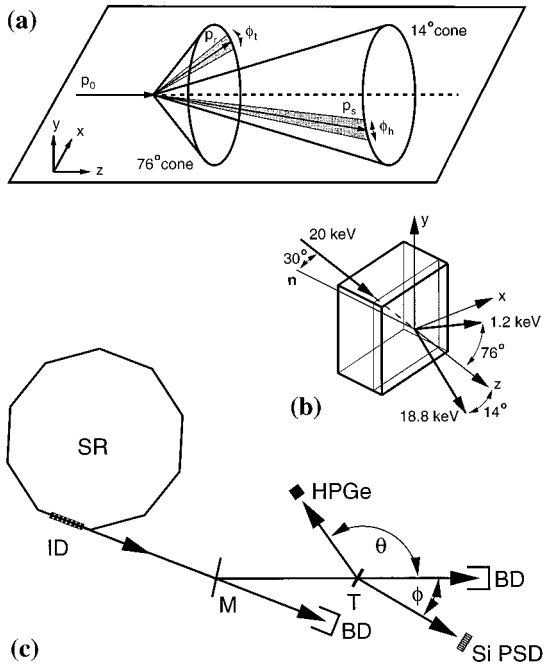

FIG. 1. (a) The experimental set up for the $(e,2e)$ reaction: the incoming beam with momentum $\mathbf{p}_0$ scatters and outgoing slow and fast electrons with momenta $\mathbf{p}_s$ and $\mathbf{p}_r$ are detected over a range of azimuthal angles ϕ_t and ϕ_h. (b) The momenta of the electrons involved relative to the target. (c) The $(\gamma,e\gamma)$ setup: SR, storage ring; ID, insertion device; M, Si(220) monochromator; T, target; HPGe, photon detector; Si PSD, electron detector; BD, beam dump.

III. EXPERIMENTS

The $(\gamma,e\gamma)$ experiment was performed at the High Energy X-Ray Scattering beamline ID 15 of the ESRF.[16] An asymmetric wiggler with 7 periods and strong poles of 1.9 T (20-mm gap) was used with a critical energy of 45 keV (Fig. 1). The white beam was monochromatized by a (220) Si crystal in Laue geometry. At an average storage ring current of 180 mA a photon flux of about 4×10^{11} photons/s at $E_0=175$ keV in a beam spot of 3 mm (horizontal)$\times$3 mm (vertical) was obtained. The monochromaticity was $\Delta E_0=650$ eV full width at half maximum (FWHM). The x-ray beam entered an evacuated target chamber (10^{-5} torr) with an externally mounted intrinsic Ge diode (energy resolution $\sim$650 eV FWHM at 122 keV) at a scattering angle $\Theta=140°$. The recoil electrons were measured by a two-dimensional (2D) array of 33 individual photodiodes, where each was equipped with its own electronic circuit (pre- and main amplifier, discriminator). The center of the array was placed at

an angle $\phi=15.2°$ relative to the primary photon momentum. At this angle, electrons with $\mathbf{q}=0$ are expected. For these electrons (i.e., those initially at rest), the scattered photon energy is $E_s=108.9$ keV and the electron recoil energy $E_r=65.6$ keV (neglecting binding energies). The array covers a range of initial electron momenta of about ± 2 a.u. The energy resolution of the photodiodes was about 7 keV (FWHM), thus worse than that of the photon branch. We therefore assumed that the modulus p_r of the recoil electron momentum could be obtained from Eq. (1) by neglecting the binding energy ϵ. The momentum transfer $K=|\mathbf{p_0}-\mathbf{p_s}|=71.6$ a.u. is very much larger than any intrinsic momentum q of the solid-state electron. The storage ring was run in the so-called $\frac{1}{3}$-fill mode, where successively one third of the buckets are filled and the following $\frac{2}{3}$ remain empty, i.e., there is light on for about 1 μs followed by a dark period of 2 μs. During ''on'' time the light is chopped on a time scale of 3 ns—the bunch distance—which is short compared to our time resolution of 200 ns. The overall coincidence count rate was about 0.15 Hz. The time-correlation spectrum showed virtually no background of accidental coincidences. The momentum resolution is different for initial electron momentum components q_z parallel to the momentum transfer vector $\mathbf{K}$ and for $q_{x,y}$ components perpendicular to $\mathbf{K}$, where q_x lies in the $(\mathbf{p}_0,\mathbf{p}_s)$ scattering plane. The resolution is in essence determined by the monochromaticity of the primary photon beam, the energy resolution of the photon detector, and the angular acceptance angles of both the photon and the electron detectors. We estimate a total error of $\Delta q_z=0.72$ a.u. (FWHM) and $\Delta q_x \cong \Delta q_y=0.88$ a.u. (FWHM).

In the $(e,2e)$ experiment, the two emerging electrons were measured in the so-called asymmetric geometry (Fig. 1): the fast electron left the backside of the foil at a scattering angle of 14° and the slow one at an angle of 76°. For a primary electron energy $E_0=20$ keV, this means that the fast electron had an energy $E_s=18.8$ keV while $E_r=1.2$ keV. In view of exchange scattering, the identification of the fast electron as the scattered one is a problem of semantics only. The same holds, of course, for the slow electron also. The two spectrometers, a hemispherical analyzer (fast electrons) and a toroidal-shaped analyzer (slow electrons) were placed in an UHV chamber (2×10^{-10} torr).[17] Electrons with pass energies of 100 eV (hemisphere) and 200 eV (toroidal) were measured with position-sensitive detectors over a range of azimuthal scattering angles: see the cones of polar angles and the range of azimuthal angles ϕ_t and ϕ_h in Fig. 1(a). The overall energy and momentum resolutions of the $(e,2e)$ experiment are estimated to be 1.0 eV and of 0.15 a.u., respectively. From the range of azimuthal angles it is deduced that the component q_y of the initial electron momentum in a direction perpendicular to the incoming electrons—parallel to the y direction indicated in Fig. 1(b)—can be determined over a range of -3.5 to $+3.5$ a.u. including the Γ point. But we should note that a systematic error in hitting the Γ point of up to 0.25 a.u. cannot be excluded due to a misalignment of the spectrometers. The momentum transfer $K=9.4$ a.u. is considerably smaller than in the $(\gamma,e\gamma)$ experiment but large enough to ensure the validity of the binary encounter approximation.[12,17] The strong enhancement of the cross section due to the asymmetric geometry compared to a symmetric geometry[17]—which maximizes the momentum transfer—allowed for beam currents less than 100 nA. The true overall coincidence count rate was a few Hz and the ratio of true to false coincidences about one. The total acquisition time was several days for each of the two experiments.

The target used was a 17-nm thin carbon foil made by laser plasma ablation.[18] The carbon atoms condensed on a thin betaine film ($C_5H_{11}NO_2\cdot H_2O$) that had a polycrystalline structure with small grains. This structure acted as a replica for the carbon film and yielded a slightly wavy character of the foil, which guaranteed rather high mechanical stability. After deposition of the carbon atoms, the betaine film was dissolved in water. In this way, a self-supporting foil with a diameter of 12 mm was obtained. Subsequently, the foil was heat treated by a short (~10-ns) pulse of a Nd:YAG laser (where YAG denotes yttrium aluminum garnet) with temperatures up to 4200 K.[18] After this treatment, electron-diffraction experiments showed sharp graphitelike patterns of randomly distributed crystallites with diameters of about 10 nm.

Since electron multiple scattering is the most severe problem in both types of experiments, we will give the mean free path for both elastic (nuclear) and inelastic scattering. The latter results mainly from plasmon excitation. From Eqs. (20) and (21) of Ref. 12, we estimate for an electron recoil energy $E_r=66$ keV in the case of the $(\gamma,e\gamma)$ experiment $\lambda_{\text{elastic}}=96$ nm and $\lambda_{\text{inelastic}}=32$ nm, whereas for $E_r=1.2$ keV in the case of the $(e,2e)$ study the corresponding values are $\lambda_{\text{elastic}}=2$ nm and $\lambda_{\text{inelastic}}=1$ nm. These values agree approximately with those estimated by Vos *et al.*[9] Since a momentum change of the recoil electron is strongly dominated by elastic scattering, we estimate from Poisson statistics that for the $(\gamma,e\gamma)$ experiment 92% of the recoil electrons leave the foil unscattered, which means that the measured EMD will be only slightly contaminated by multiple scattering, in contrast to the $(e,2e)$ experiment, where we expect rather severe elastic and inelastic multiple scattering.

IV. EXPERIMENTAL RESULTS AND DISCUSSION

First, we will give results of the $(\gamma,e\gamma)$ experiment. Roughly speaking, the q_x and q_y components of the initial electron momentum $\mathbf{q}$ are measured by the angular deviation of the emission direction of the recoil electron from the momentum transfer direction and q_z by the Doppler broadening of the scattered photons. Since the 2D electron detector covers a range of ± 2 a.u. for both q_x and q_y and the photon detector sets practically no limit for q_z, we are able to measure the complete 3D EMD all at once. Since a momentum of 1 a.u. corresponds to an angular variation of the electron-emission direction of 15 mrad only, it is necessary to use a 2D detector in order to ensure the ejection direction that corresponds to the Γ point. Figure 2 shows a 1D cut through the EMD, i.e., the coincidence count rate as a function of q_z where each panel holds for $q_y=0$ but for different q_x values. A detailed consideration[19] of the scattering kinematics reveals that q_x and q_z cannot be measured independently. For our experimental situation $q_x=q_x^0-0.13q_z$ holds, which means that in the range of -2 a.u. $<q_z<+2$ a.u. the q_z-dependent term is a small correction only. These are the q_x^0 which are quoted in the panels of Fig. 2. Note that the scale for the count rate is different for each panel, but it

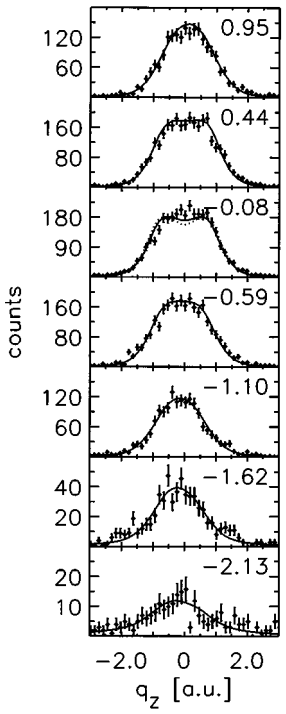

FIG. 2. Coincident photon spectra as a function of the momentum component q_z parallel to the momentum transfer vector **K**. The numbers in each panel are the component q_x^0 in a.u. (see text). The solid lines are the theory of Ref. 20.

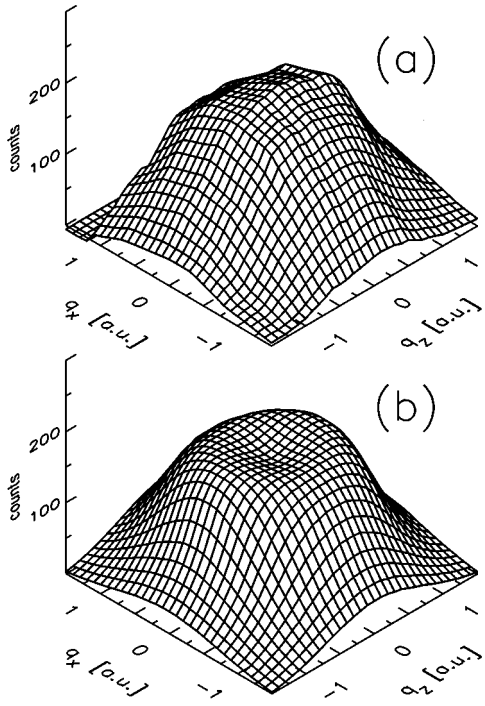

FIG. 3. (a) 2D representation of the experimental EMD from the $(\gamma,e\gamma)$ reaction for $q_y=0$. (b) The theoretical EMD from Ref. 20.

is clearly seen that the intensity falls off for increasing q_x^0. The data are compared with a theoretical EMD of graphite obtained from a pseudopotential calculation.[20] Theory has been spherically averaged to account for the isotropic nature of the foil and convoluted by the experimental resolution. In addition, theory has been corrected for the effect of multiple elastic scattering of the recoil electrons. For the 8% of scattered electrons (see above), the scattering function was obtained from a Monte Carlo calculation,[10] that simulated electron scattering and finally the theoretical EMD was folded with this distribution. Since the theoretical EMD of Ref. 20 holds for the valence electrons only, a $(1s)^2$ core contribution[21] has been added. We emphasize that theory has been fitted to the experiment by normalizing both to the same 3*D volume* in momentum space covered by the experimental data. Thus, the agreement between theory and experiment shown in Fig. 2 holds for the complete 3D data set also. The most striking feature of the EMD is the dip at $q=0$ predicted by theory and indicated by the experimental data. It results from the contribution of π electrons which are responsible for the weak van der Waals interlayer bonding along the c axis in graphite. It is the p character of these bonds from which a dip in the EMD for momenta parallel the c axis results and which survives the spherical averaging. For comparison, we have included in the panel with $q_x^0=-0.08$ a.u. of Fig. 2 the theoretical EMD without any convolution (dotted curve). The experimental data show a slightly less pronounced dip at the Γ point than in a previous experiment made with a foil that had not been treated by laser annealing,[11] but we also stress that counting statistics were about 35% better in this earlier experiment. Nevertheless, the data show an almost flat maximum for small momenta which is reminiscent of this dip. A rather strong reduction of the EMD at zero momentum has also been observed by 2D positron annihilation experiments,[22] though a quantitative comparison with our $(\gamma,e\gamma)$ experiment is not possible, since an expected positron localization in the interlayer region would give a preferred weight for annihilation with π states. For a more qualitative comparison of the $(\gamma,e\gamma)$ experimental data with theory, Fig. 3 shows a 2D cut through the data for $q_y=0$. A slight anisotropy of the data for both experiment and theory (elongation along the q_x axis) results from different experimental resolutions along q_x and q_z.

After the $(\gamma,e\gamma)$ experiment at Grenoble, the foil was transferred to Adelaide for the $(e,2e)$ investigation. Before the experiment, the foil was heated at 900 K to remove especially oxygen adsorbates from the surface. Figure 4 shows $(e,2e)$ spectra as a function of the binding energy ϵ where the value of q_y in a.u. is indicated in each panel. The reference coordinate system is now that of Figs. 1(a) and 1(b). At zero momentum the peak at about 27 eV is attributed to the σ electrons and shows the expected strong dispersion.[9,23,24] The peak at smaller binding energies—at about 10 eV—disperses only moderately and can probably be identified as resulting from the π electrons. This interpretation is at first sight at odds with the experimental observation of the low-energy peak at zero momentum, where π electrons should have vanishing intensity.[24,25] The π electrons are mostly responsible for the weak interlayer bonding in graphite and have maximum intensity along the ΓA direction of the first Brillouin zone (c-axis direction). It is the p character of this bonding that leads to the intensity of these electrons to vanish for $q=0$. Of course, this behavior also survives the spherical averaging. Since a contribution from oxygen adsor-

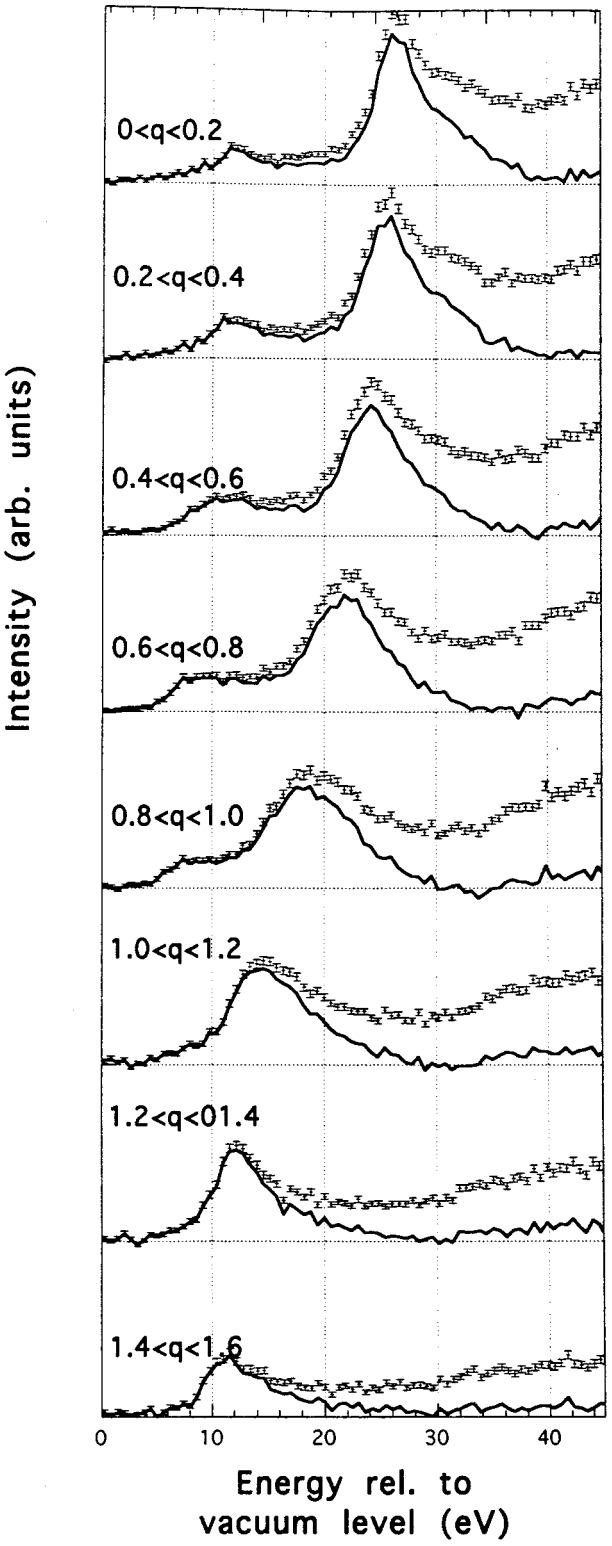

FIG. 4. Experimental $(e,2e)$ spectra (error bars) for different electron momenta q_y as indicated in each panel (in a.u.). The solid lines represent the data after a correction for multiple inelastic energy losses.

bates can be excluded, a possible explanation is the contamination of the $q_y=0$ spectrum from spectra with larger q_y due to the diffraction of one of the outgoing electrons by a reciprocal-lattice vector of a few atomic units or elastic multiple scattering effects. But we remark that Gao *et al.*[26] have given another explanation for very similar experimental findings in diamondlike amorphous carbon foils (though they do not exclude the possibility of multiple elastic scattering[12]). They also observed in their $(e,2e)$ data a strong peak at about 8 eV, which was nearly dispersionless and had the same spectral weight between $0\leqslant q\leqslant 1.7$ a.u. The observation of this peak at larger momenta q is explained by a nearly 100% sp^2 bonding also in diamondlike carbon films, contradicting the naive picture of sp^3 bonding in a diamond structure. This reasoning was confirmed by a recent tight-binding molecular-dynamics study of amorphous carbon,[27,28] which found a fraction of about 80% sp^2 bonding for a carbon density corresponding to diamondlike films produced by an ion sputtering technique. In contrast to our explanation, these authors interpret the nonvanishing intensity for $q\rightarrow 0$ as a s-p rehybridization of the π electrons arising from the loss of mirror symmetry of the twisted and wrinkled bonds in amorphous carbon films. The admixture of the s character into the π orbitals as a function of the local bending radius of the sp^2 bonds has also been discussed by Haddon *et al.*[29] We doubt if such a model would be applicable to our foil, where an investigation by electron diffraction showed sharp graphitelike rings from which we estimate an average crystalline diameter of 10 nm. Thus, due to laser annealing the status of the foil was far from being amorphous.

Since the zero point of the binding energy ϵ in Fig. 4 refers to the vacuum level, the range of the valence band in graphite extends up to about 26 eV if the Fermi level of about 5 eV is included[23,24] (the bottom of the σ band is at about 21 eV). This means that there should be no intensity in the spectra of Fig. 4 for $\epsilon>26$ eV,[30] in contrast to experimental observation. This intensity results primarily from inelastic scattering, i.e., mainly multiple plasmon excitations especially by the slow outgoing electron. The solid line in the spectra of Fig. 4 represents an attempt to deconvolute the experimental raw data according to a procedure developed by Jones and Ritter.[31]

Another interesting plot is the SEMD $\rho(\epsilon,q_y)$ as a function of q_y for ϵ as a parameter, see Fig. 5. Clearly, from the bottom of the σ band at about 26 eV one observes the splitting of the momentum distribution into two peaks, which, with decreasing binding energy, reveals the strong dispersion of the σ band. This dispersion is well reproduced quantitatively by a band structure calculation for graphite[9,24] and follows that of a nearly free-electron parabola. In the first Brillouin zone (BZ) the intensity is dominated by the s character of the σ_1 band, whereas the σ_2 and σ_3 bands have vanishing intensity due to their p character. Their intensity increases rather abruptly if the zone boundary is crossed and contributes to the intensity in the second (σ_2) and third (σ_3) BZ.[32] This behavior holds at least for symmetric directions in the basal plane but is more or less true also for other directions. After spherical averaging, all 3 σ bands contribute to the parabola in the extended-zone scheme. The sharpness of the peaks in the middle of the band at about 15–19 eV reflects the momentum resolution of about 0.15 a.u. According to theory, the intensity between the peaks should drop to zero in contradiction to the findings of Fig. 5. This is largely due to multiple elastic scattering. This scattering is quite substantial; it comprises about the same area as that in the peaks.

Spectra like those of Fig. 4 have been integrated over the

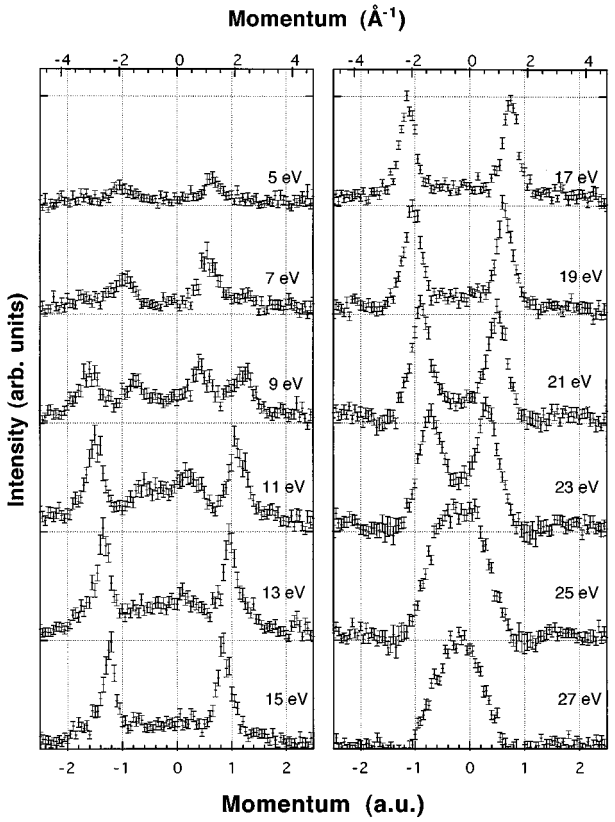

FIG. 5. Spectral momentum densities for different binding energies as indicated in each panel.

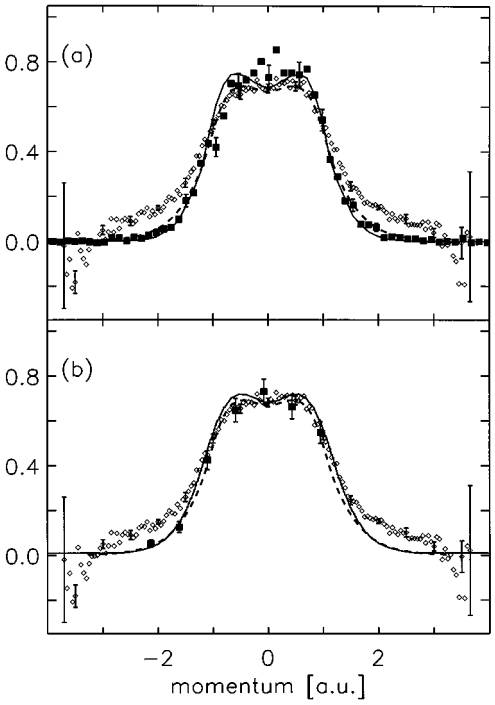

FIG. 6. Comparison of the EMD from the $(e,2e)$ experiment (open symbols) with that from the $(\gamma,e\gamma)$ reaction (closed symbols). The $(\gamma,e\gamma)$ data hold (a) for a cut along $(-0.13\ q_z,\ 0,\ q_z)$ and (b) for a cut along $(0,\ q_y,\ 0)$. In both cases the momentum plotted is the radial distance from the Γ point. The solid and broken curves are the theories of Refs. 20 and 24, respectively.

binding energy ϵ in order to get the EMD $\rho(\mathbf{q})=\int\rho(\mathbf{q},\epsilon)\,d\epsilon$, where the integration extends over the range of the valence bands only. It is evident from Fig. 4 that this can only be done for the *deconvoluted* data. In Fig. 6 the EMD from the $(e,2e)$ study (open symbols) is compared with that from the $(\gamma,e\gamma)$ experiment (closed symbols). Fig. 6(a) holds for a 1D cut of the $(\gamma,e\gamma)$ data along $(-0.13\ q_z,\ 0,\ q_z)$, Fig. 6(b) for $(0,\ q_y,\ 0)$. In order to compare with the $(e,2e)$ study, the $(\gamma,e\gamma)$ data have been corrected for the core contribution by subtracting a theoretical $(1s)^2$ EMD (Ref. 21) from the experimental result. The solid line in both figures represents the pseudopotential calculation of Lou Yongming, Johansson, and Nieminen[20] convoluted with the resolution of the $(\gamma,e\gamma)$ experiment. In addition, the broken curves show the spherically averaged EMD obtained from the linear-muffin-tin-orbital (LMTO) method based on the density-functional theory.[24] Both theories agree quite well. The slightly different curves of the pseudopotential calculation in Figs. 6(a) and 6(b) result from different resolutions of the $(\gamma,e\gamma)$ experiment in the q_z and q_y directions; see Sec. III. It demonstrates also that the convolution of this theory with the experimental resolution introduces a nearly negligible broadening only. Due to rather different granularities of the photon and electron detectors, there are, in case of the $(\gamma,e\gamma)$ experiment, far more measuring points in Fig. 6(a) (Doppler broadening in the photon detector) than in Fig. 6(b) (electron emission directions measured by the electron detector). The agreement of both sets of data is good though not perfect: the EMD of the $(e,2e)$ experiment seems to be broader than that from the $(\gamma,e\gamma)$ investigation. It is evident that this cannot be explained by the poorer resolution of the latter, since this would work in the opposite direction. Since the deconvolution procedure mentioned above accounts for *inelastic* excitations (plasmons) only, we suggest that the broadening of the $(e,2e)$ data results from multiple *elastic* scattering. In view of the complicated nature of the multiple scattering problem—elastic and inelastic scattering, both coherent (i.e., Bragg scattering) and incoherent for the incoming and outgoing electrons—we admit that the deconvolution procedure might be an intelligent guess only.[9]

Finally, we briefly address the problem of diffraction for both the incident and outgoing particles. As a measure, we give the so-called extinction length ξ_g for the excitation of a Bragg reflection at a reciprocal lattice vector $\mathbf{g}$.[33,34] Within the dynamical theory of diffraction, ξ_g reflects the penetration depth over which a considerable part of the primary intensity is diffracted (primary extinction). For the $(\gamma,\ e\gamma)$ experiment we obtain for the primary photon $\xi_{200}=0.3$ mm and for the recoil electron $\xi_{200}=20$ nm. This holds for the (200) reflection at the basal planes with $g=1.0$ a.u. The corresponding numbers for the $(e,2e)$ experiment are $\xi_{200}=10$ nm and $\xi_{200}=3$ nm for the primary and recoil electrons, respectively. This estimate demonstrates that diffraction effects in the case of the $(e,2e)$ experiment can be of considerable influence. A first attempt to account for this effect was undertaken by Allen *et al.*[35]

V. SUMMARY AND PERSPECTIVES

We have compared the electron momentum densities for polycrystalline graphite foils obtained by $(\gamma,e\gamma)$ and $(e,2e)$

spectroscopy and found reasonable agreement. For the $(\gamma,e\gamma)$ experiment, the recoil electron energy was high enough to suppress almost quantitatively both elastic and inelastic multiple electron scattering within the target. The small scattering cross section (Klein-Nishina) and small photon fluxes resulted in rather poor energy and momentum resolutions compared to the $(e,2e)$ investigation. The asymmetric scattering geometry in the latter case guaranteed a large Møller cross section but also led to strong electron multiple-scattering effects. In this connection, we note that the cross-section ratio 5×10^5 in favor of the $(e,2e)$ experiment quoted in the Introduction is reduced by at least a factor of 10, since the whole target thickness (17 nm) does not contribute effectively to the coincidence count rate but only the last mean free path for scattering ($\sim$2 nm). Nevertheless, the comparison has demonstrated that solid-state EMD's can be obtained by both methods with reasonable accuracy.

How can the experiments be improved? For the photon experiment we plan to use a multipixel 2D photon detector in place of the single-pixel Ge diode. In addition, there is the possibility of using the synchrotron radiation beamline at the 12-GeV PETRA storage ring at DESY, Hamburg.[11] At photon energies of about 180 keV we expect for this undulator beamline an increase of photon flux of about 100, which could be used to improve the resolution of the experiment. For the $(e,2e)$ experiment the multiple-scattering problem could strongly be reduced by going to higher primary electron energies. For $E_0=100$ keV and a symmetric geometry (i.e., a scattering angle of 43.7° for both outgoing electrons and $E_s=E_r=50$ keV), the Møller cross section is reduced to 8 b/sr/electron, i.e., by a factor of 2×10^3 (effectively, it is only a factor of 100, since now the whole foil contributes to the coincidences, a conclusion also reached by Dennison and Ritter[12]). Nevertheless, it might be that such an experiment is feasible without loosing too much resolution.[12]

ACKNOWLEDGMENTS

We thank Günther Dollinger and Peter Meier-Komor from the Target Laboratory of the Technical University of Munich for the graphite foil and Vejo Honkimäki from the University of Helsinki, Finland, for his help during the beam time at the ESRF. The $(\gamma,e\gamma)$ experiment was supported by the Bundesministerium für Bildung, Wissenschaft, Forschung und Technologie under Contract Nos. 05 5 WMAAI and 05 650 WEA. The Electronic Structure of Materials Centre, Adelaide, is supported by a grant of the Australian Research Council.

*Electronic address: kurp@desy.de
†Present address: Research School of Physical Sciences and Engineering, Australian National University, Canberra, ACT 2601, Australia.

[1] I. Schäfer, M. Schlüter, and M. Skibowski, Phys. Rev. B **35**, 7663 (1987).
[2] H. Nishimoto, T. Nakatani, T. Matsushita, S. Imada, H. Daimon, and S. Suga, J. Phys. Condens. Matter **8**, 2715 (1996).
[3] W. Schülke, U. Bonse, N. Nagasawa, A. Kaprolat, and A. Berthold, Phys. Rev. B **38**, 2112 (1988).
[4] B. M. Kincaid, A. E. Meixner, and P. M. Platzman, Phys. Rev. Lett. **40**, 1296 (1978).
[5] P. Skytt, P. Glans, D. C. Mancini, J.-H. Guo, N. Wassdahl, J. Nordgren, and Y. Ma, Phys. Rev. B **50**, 10 457 (1994).
[6] R. Chen, P. Trucano, and R. F. Stewart, Acta Crystallogr. Sect. A **33**, 823 (1977).
[7] I. Kanazawa, S. Tanigawa, R. Suzuki, M. Sano, and H. Inokuchi, Phys. Rev. B **42**, 11 583 (1990).
[8] M. J. Puska and R. M. Nieminen, Rev. Mod. Phys. **66**, 841 (1994).
[9] M. Vos, P. Storer, S. A. Canney, A. S. Kheifets, I. E. McCarthy, and E. Weigold, Phys. Rev. B **50**, 5635 (1994).
[10] Th. Tschentscher, J. R. Schneider, and F. Bell, Phys. Rev. B **48**, 16 965 (1993).
[11] F. F. Kurp, Th. Tschentscher, H. Schulte-Schrepping, J. R. Schneider, and F. Bell, Europhys. Lett. **35**, 61 (1996).
[12] J. R. Dennison and A. L. Ritter, J. Electron. Spectrosc. Relat. Phenom. **77**, 99 (1996).
[13] M. Vos and I. E. McCarthy, Rev. Mod. Phys. **67**, 713 (1995).
[14] P. Eisenberger and P. M. Platzman, Phys. Rev. **2**, 415 (1970).
[15] R. S. Caprari, S. A. C. Clark, I. E. McCarthy, P. J. Storer, M. Vos, and E. Weigold, Phys. Rev. B **50**, 12 078 (1994).
[16] P. Suortti and Th. Tschentscher, Rev. Sci. Instrum. **66**, 1798 (1995).
[17] P. Storer, S. A. C. Clark, R. C. Caprari, M. Vos, and E. Weigold, Rev. Sci. Instrum. **65**, 2214 (1994).
[18] G. Dollinger and P. Maier-Komor, Nucl. Instrum. Method. A **303**, 50 (1991).
[19] F. F. Kurp, A. E. Werner, J. R. Schneider, Th. Tschentscher, P. Suortti, and F. Bell, Nucl. Instrum. Methods (to be published).
[20] Lou Yongming, B. Johansson, and R. M. Nieminen, J. Phys. Condens. Matter **3**, 1699 (1991).
[21] E. Clementi and C. Roetti, At. Data Nucl. Data Tables **14**, 177 (1974).
[22] R. R. Lee, E. C. von Stetten, M. Hasegawa, and S. Berko, Phys. Rev. Lett. **58**, 2863 (1987).
[23] J.-C. Charlier, X. Gonze, and J.-P. Michenaud, Phys. Rev. B **43**, 4579 (1991); J.-C. Charlier, J.-P. Michenaud, and X. Gonze, *ibid.* **46**, 4531 (1992).
[24] A. S. Kheifets and M. Vos, J. Phys. Condens. Matter **7**, 3895 (1995).
[25] A. S. Kheifets, J. Lower, K. J. Nygaard, S. Utteridge, M. Vos, and E. Weigold, Phys. Rev. B **49**, 2113 (1994).
[26] C. Gao, Y. Y. Wang, A. L. Ritter, and J. R. Dennison, Phys. Rev. Lett. **62**, 945 (1989).
[27] C. Z. Wang, K. M. Ho, and C. T. Chan, Phys. Rev. Lett. **70**, 611 (1993); Phys. Rev. B **47**, 14 835 (1993)
[28] G. Galli, R. M. Martin, R. Car, and M. Parrinello, Phys. Rev. Lett. **62**, 555 (1989); Phys. Rev. B **42**, 7470 (1990).
[29] R. C. Haddon, L. E. Brus, and K. Raghavachari, Chem. Phys. Lett. **131**, 165 (1986).
[30] M. Vos, P. Storer, A. S. Kheifets, I. E. McCarthy, and E. Weigold, J. Electron. Spectrosc. Relat. Phenom. **76**, 103 (1995).
[31] R. Jones and A. Ritter, J. Electron. Spectrosc. Relat. Phenom. **40**, 285 (1986).
[32] Chao Gao, A. L. Ritter, J. R. Dennison, and N. A. W. Holzwarth, Phys. Rev. B **37**, 3914 (1988).

[33] L. Reimer, *Transmission Electron Microscopy*, Springer Series in Optical Sciences Vol. 36 (Springer-Verlag, Berlin, 1984), p. 279.

[34] M. v. Laue, *Röntgenstrahlinterferenzen* (Akademische Verlagsgesellschaft, Frankfurt am Main, 1960).

[35] L. J. Allen, I. E. McCarthy, V. W. Maslen, and C. J. Rossouw, Aust. J. Phys. **43**, 453 (1990); L. J. Allen and C. J. Rossouw, Phys. Rev. B **47**, 2446 (1993).